A Scale-Discriminating Vorticity Budget for a Mesoscale Vortex in a Midlatitude, Continental Mesoscale Convective System

JASON C. KNIEVEL

National Center for Atmospheric Research, Boulder, and Department of Atmospheric Science, Colorado State University, Fort Collins, Colorado

RICHARD H. JOHNSON

Department of Atmospheric Science, Colorado State University, Fort Collins, Colorado

(Manuscript received 18 January 2002, in final form 23 September 2002)

ABSTRACT

The authors employ data from the NOAA Wind Profiler Network to present a scale-discriminating vorticity budget for a mesoscale convective vortex (MCV) that was generated by a mesoscale convective system (MCS) in Oklahoma and Kansas on 1 August 1996.

A spatial bandpass filter was used to divide observed wind into mesoscale and synoptic components. Then the authors sought sources and sinks of vorticity in those two components over 9 h of the MCV's lifetime.

The vorticity budget reveals that both the mesoscale and synoptic winds supplied significant vorticity to the MCV. The vortex's origin could not be proved, but data weakly suggest that tilting may have been mostly responsible. Convergence of absolute vorticity by the mesoscale wind was the reason the MCV grew deeper and stronger as the MCS weakened. Finally, tilting of synoptic and mesoscale vorticity by gradients in mesoscale vertical motion was responsible for a secondary deepening of the MCV as the MCS dissipated.

The budget suggests that, if the MCV of 1 August 1996 is representative, completely realistic simulations of MCVs should include planetary vorticity and a plausible, three-dimensionally heterogeneous synoptic wind.

1. Introduction

In this paper we present a vorticity budget for a mesoscale convective vortex (MCV) generated by a mesoscale convective system (MCS) that traversed Kansas and Oklahoma on 1 August 1996. The budget discriminates between sources and sinks of vorticity within the mesoscale wind of the MCS and within the synoptic background wind.

a. Background

MCSs often generate MCVs in the lower and middle troposphere. An MCV's tangential wind speed is of orders 1 and 10 m s^{-1}, its diameter of order 100 km, and its lifetime of orders 1 and 10 h. MCVs organize MCSs on the mesoscale (Menard and Fritsch 1989; Brandes 1990) and can serve as the primary dynamical link among serial MCSs (Raymond and Jiang 1990; Fritsch et al. 1994; Trier et al. 2000).

If friction is ignored, vertical vorticity within an MCV must originate from some combination of (a) horizontal advection of absolute vorticity, (b) vertical advection of relative vorticity, (c) convergence of absolute vorticity, (d) tilting of horizontal vorticity by horizontally varying vertical wind, and (e) horizontal baroclinity. This is apparent upon examination of the equation for the local change in relative vertical vorticity of an inviscid fluid on an f plane:

$$\frac{\partial \zeta}{\partial t} = \underbrace{-[\mathbf{v}\cdot\nabla(\zeta + f)]}_{a} \underbrace{- \left(w\frac{\partial \zeta}{\partial z}\right)}_{b} \underbrace{- [(\zeta + f)\nabla\cdot\mathbf{v}]}_{c} + \underbrace{\left(\xi\frac{\partial w}{\partial x} + \eta\frac{\partial w}{\partial y}\right)}_{d} + \underbrace{[\mathbf{J}_{xy}(p, \alpha)]}_{e}, \quad (1)$$

wherein $\boldsymbol{\zeta}(\xi, \eta, \zeta)$ is relative vorticity, $\mathbf{v}(u, v)$ is horizontal wind, w is vertical wind, f is the Coriolis parameter, and $\mathbf{J}_{xy}(p, \alpha)$ is the two-dimensional Jacobian of pressure, p, and specific volume, α. (Letters assigned to the terms correspond to the enumeration earlier in the paragraph.) Baroclinity is weak near MCVs and can be ignored without losing much accuracy (Skamarock et al. 1994; Cram et al. 2002). (Henceforth, *vorticity*

Corresponding author address: Dr. Jason Knievel, NCAR, P.O. Box 3000, Boulder, CO 80307-3000.
E-mail: knievel@ucar.edu

means relative vertical vorticity, and *divergence, convergence,* and *shear* mean horizontal divergence, horizontal convergence, and vertical shear, unless otherwise stated.) In a Lagrangian sense, advections only redistribute vorticity, they do not create it, so analyses of vorticity in MCVs tend to emphasize divergence and tilting, terms (c) and (d) in (1). Contributions from both sources frequently are large (e.g., Brandes 1990; Chong and Bousquet 1999).

A positive contribution to vorticity can come from convergence in the middle troposphere within the stratiform region of an MCS, where existing planetary and synoptic vorticity can be concentrated (Bartels and Maddox 1991; Johnson and Bartels 1992; Skamarock et al. 1994). Some of this convergence is due to the atmosphere's balanced response to heating and cooling by phase changes in water within the stratiform region of an MCS (Hertenstein and Schubert 1991). The strength of this balanced response depends on the Rossby radius of deformation:

$$\lambda_R = \frac{NH}{(\zeta + f)^{1/2}(2VR^{-1} + f)^{1/2}}, \qquad (2)$$

wherein N is the Brunt–Väisällä frequency, H is the scale height of the disturbance, ζ is the vertical component of relative vorticity, f is the Coriolis parameter, and V is the wind's rotational component, of which R is radius of curvature (Schubert et al. 1980; Frank 1983). It is generally appropriate to choose values for N, ζ, f, and V that are averaged over the region diabatically heated by moist convection. In an environment of 100% relative humidity, rising air is heated by condensation as well as cooled by expansion, so N should be replaced by N_m, as explained by Durran and Klemp (1982). When sources of diabatic heating are larger than λ_R, more energy is retained in balanced, vortical flow near an MCS than is transmitted to the far field by gravity waves and buoyancy rolls; the opposite occurs when sources of diabatic heating are smaller than the Rossby radius (Schubert et al. 1980; Mapes 1993). An MCS can shrink its local Rossby radius by saturating the stratiform region, which means that a potentially lower-valued N_m replaces N, and by generating a vortical circulation, which increases $2VR^{-1}$ (Schubert and Hack 1982; Cotton et al. 1989; Chen and Frank 1993).

Tilting's positive contribution can come from horizontally varying vertical motion in an MCS's mesoscale updraft or downdraft that tilts vorticity equated with vertically and horizontally sheared wind (Davis and Weisman 1994). Shear exists in both the wind of an MCS and the wind of the system's environment, but initial studies of tilted vorticity in MCVs emphasized only environmental shear (e.g., Biggerstaff and Houze 1991) or did not formally differentiate between the two shears (e.g., Brandes 1990; Zhang 1992). More recent studies demonstrated that vertical shear in MCSs is also an important source of vorticity within MCVs (e.g., Chong and Bousquet 1999; Bousquet and Chong 2000).

b. Objective and motivation

Most empirical vorticity budgets for MCVs fall into two categories. In the first are studies of vorticity on the scale of an MCS and MCV; these are usually based on Doppler radars and/or research sounding networks (e.g., Biggerstaff and Houze 1991; Johnson and Bartels 1992; Chong and Bousquet 1999). In the second are larger-scale budgets based on the nation's operational sounding network (e.g., Bartels and Maddox 1991). Studies in both categories are usually valid only for a few hours or for a single stage of an MCV because of the difficulty of obtaining detailed kinematical data over a substantial fraction of an MCV's lifetime.

Before now, no empirical vorticity budget for an MCV simultaneously investigated circulations within an MCS as well as those within the MCS's larger-scale environment. The MCV of 1 August 1996 presented an opportunity for just such an investigation when the vortex spent the majority of its lifetime within the densest part of the National Oceanic and Atmospheric Administration (NOAA) Wind Profiler Network. In a closely related paper (Knievel and Johnson 2002), we examined the life cycle and kinematics of the MCS that generated the MCV. Our objective in this paper is to extend that research by presenting for an MCV the first vorticity budget that explicitly comprises terms for sources and sinks of vorticity within an MCS, its environment, and combinations of the two. The budget has the added advantage of encompassing 9 h of the MCV's lifetime.

2. Data and methods

Observations are from the National Weather Service (NWS), remote sensors operated by NOAA, the 1996 Enhanced Seasonal Observing Period (ESOP-96) of the Global Energy and Water Cycle Experiment's (GEWEX's) Continental-Scale International Project (GCIP), and the Oklahoma Climatological Survey's Oklahoma Mesonet (Brock et al. 1995).

The previously published kinematical analysis of the MCS of 1 August 1996 (Knievel and Johnson 2002) provides details about the data and some of our methods, so herein we emphasize only the methods integral to understanding the vorticity budget and related calculations.

a. Objective analyses and bandpass filtering

To produce gridded fields of total wind, $\mathbf{u}$ (u, v, w), we used a two-pass Barnes analysis (Barnes 1973; Koch et al. 1983) on data from the NOAA Wind Profiler Network (NPN; Fig. 1). Grid points were 75 km apart, the cutoff radius was 750 km, and the response function was chosen to capture 90% of the signal of phenomena with wavelengths of 300 km, which is twice the average distance between profilers in the densest part of the NPN (*total* curve in Fig. 2). Less than 10% of the signal of

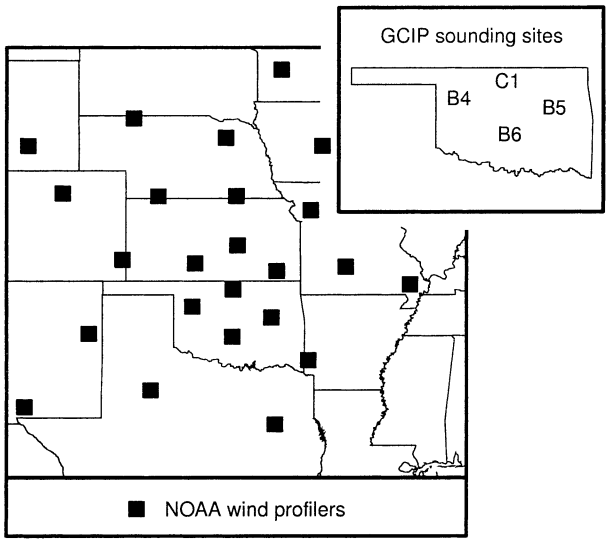

FIG. 1. Sites of observations above the ground. NOAA wind profilers are marked by black squares. The inset box shows the locations of GCIP sounding sites.

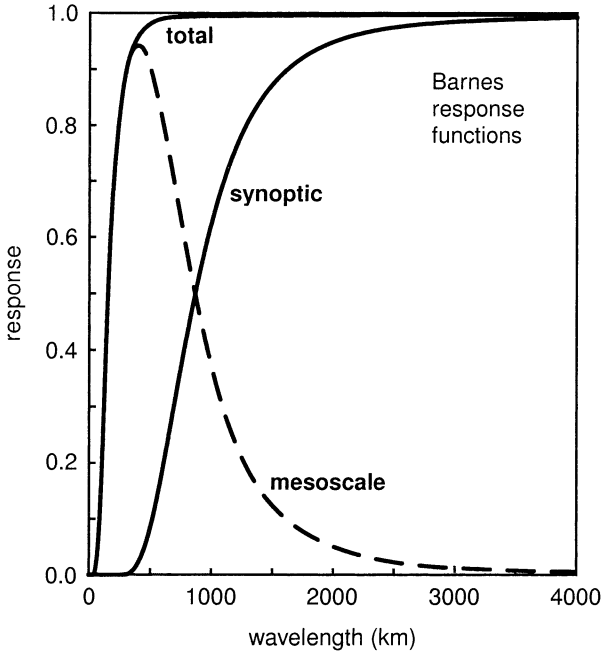

FIG. 2. Response functions of the Barnes analyses.

phenomena with wavelengths shorter than 85 km was captured, so virtually no coherent convective signal exists in the analyzed data.

To isolate partially the mesoscale kinematics of the MCS from the synoptic kinematics, we employed a second Barnes analysis that, together with the first, acted as a bandpass filter (Maddox 1980). The synoptic background wind, $\tilde{\mathbf{u}}(\tilde{u}, \tilde{v}, \tilde{w})$, was approximated with data filtered to include 90% and 0.09% of the signals of phenomena with wavelengths of 1600 and 300 km, respectively (*synoptic* curve in Fig. 2). This is the same filtration that Maddox (1980) used for synoptic features. The mesoscale perturbation in wind, $\hat{\mathbf{u}}(\hat{u}, \hat{v}, \hat{w})$, was approximated by subtracting the synoptic background wind from the total wind (*mesoscale* curve in Fig. 2). In summary, $\mathbf{u}(u, v, w) = \tilde{\mathbf{u}}(\tilde{u}, \tilde{v}, \tilde{w}) + \hat{\mathbf{u}}(\hat{u}, \hat{v}, \hat{w})$.

The bandpass filter did not completely isolate the mesoscale and synoptic winds from each other, especially at scales near where the two response curves cross (Fig. 2). However, the wavelengths of the MCS and MCV of 1 August 1996 were near the peak of the mesoscale response function, ~400 km, where the synoptic part of the filter was quite insensitive.

b. Divergence, vorticity, and vertical velocity

Calculations of divergence and vorticity are from centered finite differences of objectively analyzed fields of u and v components of the wind. We found this method sufficiently accurate when tested against line integrals of tangential and normal components of wind calculated around the perimeter of triangles whose vertices were the profilers (Ceselski and Sapp 1975). Vertical velocity is from the kinematical method with a linear correction to density-weighted divergence (O'Brien 1970), wherein $w = 0$ at 1000 m above the tropopause and at 500 m above ground level (AGL).

c. Averages over the stratiform region

Although the NPN provided a much more resolved dataset than would have been available from operationally launched radiosondes alone, missing data still made it impossible to perform detailed hourly analyses at every grid point because large spatial gaps greatly reduced the accuracy of the Barnes analyses at a few individual times. We mitigated this problem by examining objectively analyzed data that were then temporally and spatially averaged over 3 h and a $2° \times 2°$ area centered on the MCV, whose radius of maximum wind was approximately 0.75°–1.50° latitude (83–167 km).

Official observations from the NPN for a time t are of wind recorded over the hour ending at t. So, for example, an average of NPN observations from 1000, 1100, and 1200 UTC, such as we calculated, is an average of wind recorded from 0901 to 1200 UTC.

d. Vorticity budget

As mentioned in section 1, for a vorticity budget of wind above the boundary layer and any cold pools, it is reasonable to dismiss baroclinity, represented by the Jacobian in (1). The remaining four terms in (1) were retained for the budget.

For our case, the local derivative on the left side of (1) is for a $2° \times 2°$ area repositioned every hour so it was centered on the midtropospheric part of the MCV. Mesoscale wind in the middle troposphere was virtually

the same as a system-relative wind (i.e., wind in a frame of reference that moved with the MCV) because the translational motion of the MCV was due primarily to advection by the background synoptic wind in the middle troposphere, which is common (e.g., Zhang and Fritsch 1988; Johnson and Bartels 1992; Trier et al. 2000). Over the detectable lifetime of the MCV, zonal and meridional components of the synoptic background wind at the three-dimensional center of the MCV were 7.7 and -8.1 m s^{-1}, respectively. The corresponding components of the MCV's average translational velocity were 7.4 and -8.1 m s^{-1}. Therefore, once the synoptic wind was removed from the total wind, the frame of reference moved in the middle troposphere with the MCV, and the circulation of the mesoscale perturbation in wind within the MCV was approximately closed (Knievel and Johnson 2002).

We calculated on a grid the vorticity budget for the mesoscale perturbation in wind, for the synoptic background wind, and for the sum of the two, the total wind. This sum is not truly a total wind in that it does not contain fully sampled contributions from subgrid phenomena such as eddies from cumulonimbi. First, the NPN is insufficiently dense to record unaliased observations of such phenomena. Second, filtering by the Barnes routine excluded nearly all sources and sinks of vorticity with wavelengths smaller than 85 km. Yet phenomena this small undoubtedly contributed to temporal changes in vorticity (Weisman and Davis 1998), and those contributions probably translated to larger scales to which the Barnes routine was sensitive (Esbensen 1993). Fortunately, eddy fluxes of momentum in MCSs are generally less in stratiform regions than in convective lines (Gallus and Johnson 1992), and our vorticity budget is limited to the former.

Because of such unresolved sources and sinks of vorticity, the vorticity budget has a residual, which also includes observational errors. When written in terms of the resolved synoptic component [designated by $(\tilde{\ })$], the resolved mesoscale component [designated by $(\hat{\ })$], and the residual Z, (1) becomes

$$\frac{\partial\zeta}{\partial t} = -(\tilde{\mathbf{v}} + \hat{\mathbf{v}})\cdot\nabla(\tilde{\zeta} + f + \hat{\zeta}) - (\tilde{w} + \hat{w})\frac{\partial(\tilde{\zeta} + \hat{\zeta})}{\partial z} - (\tilde{\zeta} + f + \hat{\zeta})\nabla\cdot(\tilde{\mathbf{v}} + \hat{\mathbf{v}}) + (\tilde{\xi} + \hat{\xi})\frac{\partial(\tilde{w} + \hat{w})}{\partial x} + (\tilde{\eta} + \hat{\eta})\frac{\partial(\tilde{w} + \hat{w})}{\partial y} + \mathbf{J}_{xy}(\tilde{p} + \hat{p}, \tilde{\alpha} + \hat{\alpha}) + Z. \quad (3)$$

We vertically smoothed terms in the budget with a five-point, center-weighted running mean.

Often the resolved terms on the right side of a budget that is in the form of (3) together nearly cancel the residual, leaving the local tendency as a small difference in this near cancellation (e.g., Reed and Johnson 1974). Therefore, the magnitude and even the sign of the local tendency, $\partial\zeta/\partial t$, is very sensitive to errors in the horizontal derivatives that compose the resolved terms. This sensitivity is especially troublesome if one uses the local tendency to predict vorticity. We made no such predictions because observations of vorticity were available every hour for our analysis. Even so, it is valuable to assess how the resolvable part of the local tendency differs when calculated with a budget based on a mathematically simpler form of the vorticity equation than the form on which we based (3).

One such equation, used in vorticity budgets by Davis and Weisman (1994) and Weisman and Davis (1998), among others, may be written most succinctly as

$$\frac{\partial\zeta}{\partial t} = \nabla\cdot\mathbf{K}, \quad (4)$$

in which friction and baroclinity are ignored, and

$$\mathbf{K} = w\left(\mathbf{k}\times\frac{\partial\mathbf{v}}{\partial z}\right) - \mathbf{v}(\zeta + f), \quad (5)$$

wherein $\mathbf{k}$ is the vertical unit vector and all the other symbols have meanings as in (3). When (4) and (5) are combined, the explicit terms are

$$\frac{\partial\zeta}{\partial t} = -\frac{\partial}{\partial x}\left[w\frac{\partial v}{\partial z} + u(\zeta + f)\right] - \frac{\partial}{\partial y}\left[w\frac{\partial u}{\partial z} + v(\zeta + f)\right]. \quad (6)$$

We checked the results of (3), which we call the conventional form of the vorticity budget, with (4), which is sometimes called the flux form, but which we call the divergence form of the vorticity budget. Results of the check appear in section 5.

e. Rossby radius of deformation

Calculations of the Rossby radius of deformation, λ_R, were hampered by scant thermodynamical data. One of only two GCIP radiosondes from which data were not lost during penetration of the stratiform region was launched at 1800 UTC from Morris, Oklahoma (B5). From that sounding (not shown) we calculated N in (2) over a depth of 3 km to be 1.05×10^{-2} s^{-1}, which we used in calculations for the stratiform region at other times. The resultant value of 31.5 m s^{-1} for NH is very close to the fixed 30.0 m s^{-1} used by Cotton et al. (1989) in their evaluation of changes in λ_R over the lifetime of a composite mesoscale convective complex (MCC), a specific type of large MCS. Although our calculation of λ_R was for a part of the stratiform region, the lower troposphere was subsaturated there, so we used N instead of the N_m mentioned in section 1a.

3. Overview of vorticity in the MCS and MCV

The MCS, which comprised a leading convective line and a trailing stratiform region, formed at 0430 UTC on 1 August 1996 and had completely dissipated by 0315 UTC on 2 August (Knievel and Johnson 2002). The first sign of an MCV was at 0715 UTC on 1 August, and by 0315 UTC on 2 August the MCV was no longer detectable in radar, satellite, or profiler data. Figure 3 depicts the MCS as it appeared in composite radar summaries. Even in these static schemata, little imagination is needed to envision the vortical flow that defined the MCV and shaped the MCS's stratiform region.

Over the 9 h we examined, 0900 to 1800 UTC on 1 August (which we call the period of detailed analysis), the MCV deepened and strengthened as the MCS matured and dissipated. Eventually the vortex occupied almost the entire troposphere, perhaps even reaching the ground (Knievel and Johnson 2002).

Positive vorticity in the MCV seemed to originate at about 3 km above mean sea level (AMSL), in a nondivergent layer of weak ascent (Fig. 4), and from 0900 to 1200 UTC this was approximately the altitude of its average maximum vorticity (Fig. 5a). Then the top of the vortex and the level of maximum vorticity both ascended between 1200 and 1500 UTC (Fig. 5b) as the vortex strengthened and the stratiform region dominated the MCS, judging from the profile of vertical motion (Houze et al. 1989). After these ascensions, the altitude of maximum vorticity remained approximately fixed at 6 km AMSL for the remainder of the period of detailed analysis, during which time the vortex's top reached 13 km AMSL (Fig. 5c).

The long-lived simulated MCV of Zhang and Fritsch (1988) behaved similarly: the height of maximum vorticity varied little for the first 2 h of the MCV's life, rose quickly as the MCV strengthened, then varied little after that. Conversely, Chen and Frank (1993) simulated an MCV whose vorticity maximum descended, not ascended, with time. Few empirical studies recount temporal variations of vorticity within an MCV, but among these few Menard and Fritsch (1989) did find that maximum vorticity ascended with time in the MCV of 6–7 July 1982, which was the MCV simulated by Zhang and Fritsch (1988).

The MCV of 1 August 1996 was deeper than many MCVs, but not all. The simulated MCVs of Chen and Frank (1993) and Rogers and Fritsch (2001), respectively, had tops near and above 200 hPa. (In our case, 200 hPa was approximately 12.4 km AMSL.) The observed MCVs of Brandes (1990) and Bousquet and Chong (2000) had tops near 11 km AMSL.

The shallow, weak, negative vorticity above the mature MCV of 1 August 1996 (Fig. 5c) is the signature of planetary vorticity's effect on divergent outflow from high pressure in the upper troposphere (e.g., Brandes 1990; Johnson and Bartels 1992; Bousquet and Chong 2000).

A more thorough discussion of divergence and vertical motion within the MCV appeared in our earlier paper (Knievel and Johnson 2002). Please see it for more detailed commentary on Fig. 5.

4. Vorticity budget

According to our application of (3), convergence, tilting, and unresolved effects contributed the most to net changes in the MCV as it matured, and prominent sources and sinks of vorticity existed in both the synoptic and mesoscale components of the wind. (The vorticity, divergence, and vertical motion presented in Fig. 5 may aid in the interpretation of the budget in the following section.)

a. Total wind

In the total wind, there were only two positive sources of vorticity in the lower troposphere at the altitude of the developing MCV between 0900 and 1200 UTC: tilting (Fig. 6b) and unresolved effects (Fig. 7). Because the vortex had already formed by the start of the period of detailed analysis, we could not conclusively determine the source of vorticity in the incipient vortex. Even so, Fig. 6b weakly suggests that tilting may have played the largest role on resolved scales, which would be consistent with the study by Zhang (1992), whose simulated MCV began primarily from tilting, then in maturity strengthened from convergence.

The MCV of 1 August 1996 grew deeper and stronger between 1200 and 1500 UTC, primarily from convergence of positive absolute vorticity in the middle troposphere (Fig. 6c). Planetary and relative vorticities contributed almost equally (not shown). If not for divergence of planetary vorticity in the upper troposphere, the tendency due to divergence there at 1500 UTC would have been positive as well, because upper-tropospheric relative vorticity was negative (Fig. 5b). Indeed, because divergence and relative vorticity were roughly anticorrelated about zero in the middle and upper troposphere (Fig. 5b), any deep layers of strongly negative tendency due to divergence at those altitudes must have been from divergent wind acting on planetary vorticity, because divergence of negative relative vorticity and convergence of positive relative vorticity cannot produce a negative tendency. Davis and Weisman (1994) alluded to this. At the same time that convergence of absolute vorticity generated relative vorticity in the lower and middle troposphere, the mesoscale updraft advected that vorticity upward (Fig. 6d). However, positive vertical advection of vorticity was overwhelmed by all the other resolved sinks. In particular, horizontal advection decreased vorticity from the lower through the upper troposphere, which is partly a result of the way vorticity was averaged; as long as the $2^\circ \times 2^\circ$ area of averaging remained centered on the maximum vorticity in the MCV, any horizontal advection into or

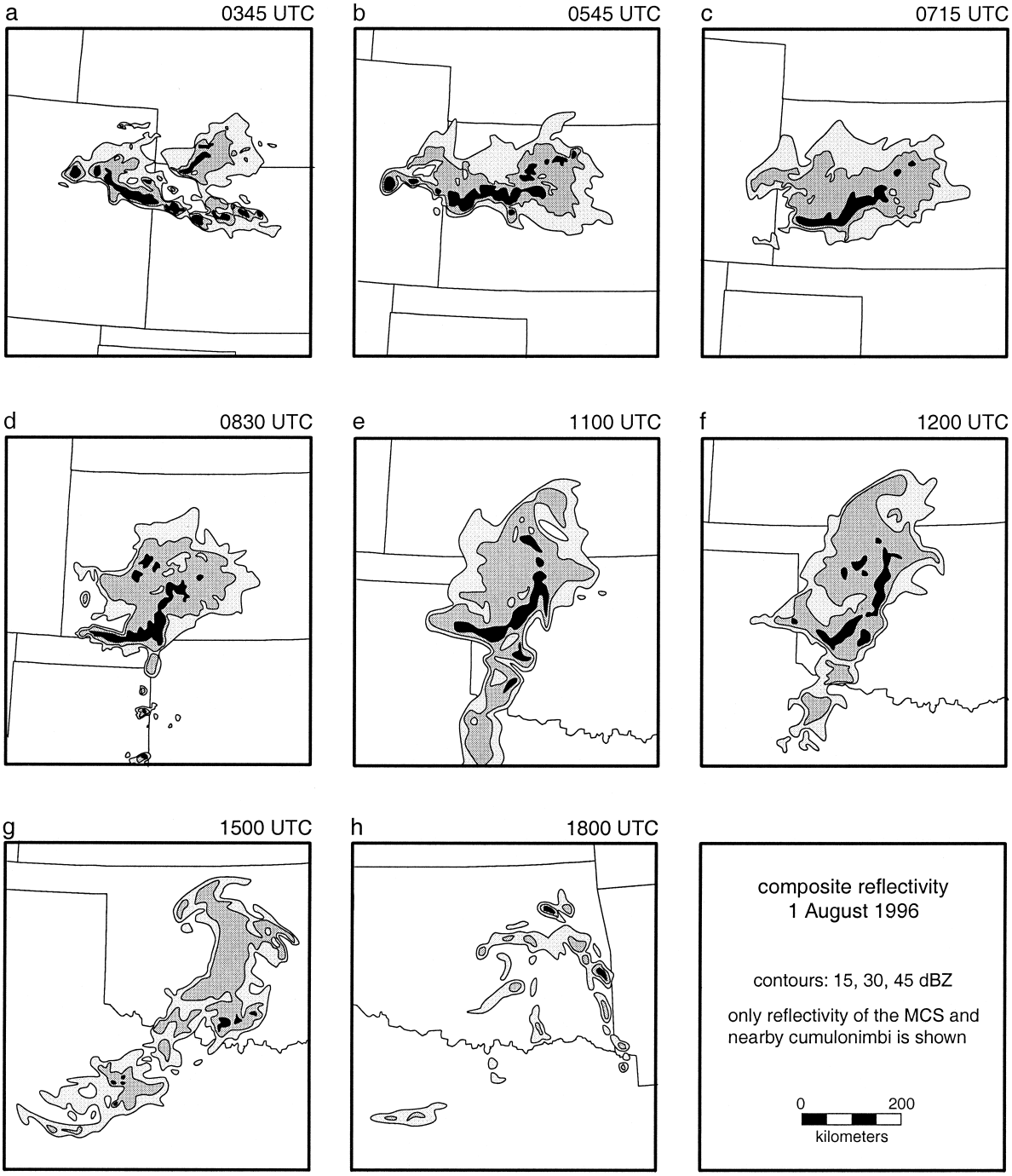

FIG. 3. Schemata of composite base-scan radar reflectivity on 1 Aug 1996. Times are (a) 0345, (b) 0545, (c) 0715, (d) 0830, (e) 1100, (f) 1200, (g) 1500, and (h) 1800 UTC. Contours are at 15, 30, and 45 dBZ. Only reflectivity due to the MCS and nearby cumulonimbi is shown.

out of that area would necessarily produce a negative tendency. At 1500 UTC, sources that compose part of the residual appear to have acted in concert with vertical advection above the MCV but at the altitude of the MCV strongly opposed the positive tendency from convergence (Fig. 7).

Convergence of absolute vorticity between 1200 and 1500 UTC was likely aided by the existent MCV. As explained in section 1a, when sources of diabatic heating are larger than the Rossby radius of deformation, λ_R, more energy is retained in balanced, vortical flow near an MCS than is transmitted to the far field by gravity waves and buoyancy rolls (Mapes 1993; Schubert et al. 1980). The transition to such balanced, vortical flow

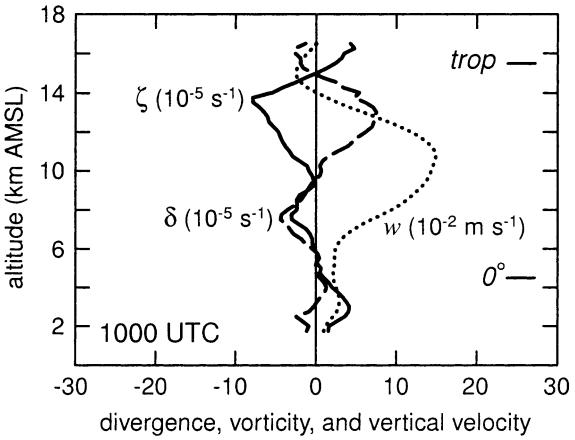

FIG. 4. Relative vorticity (solid, in 10^{-5} s^{-1}), divergence (dashed, in 10^{-5} s^{-1}), and vertical velocity (dotted, in 10^{-2} m s^{-1}) of the total wind at 1000 UTC 1 Aug 1996. Profiles are for a 2° × 2° area centered on the MCV. Unlike in Fig. 5, profiles are not for 3-h averages. Data below 1750 m AMSL are not plotted. The levels of 0°C in the environment and of the tropopause are marked along the right side.

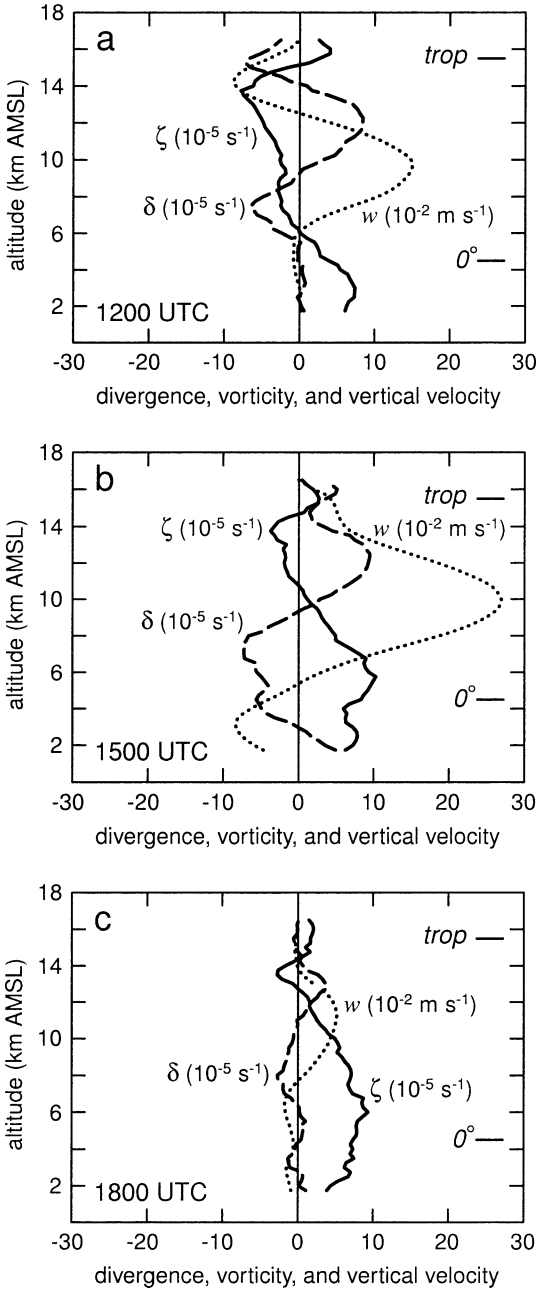

FIG. 5. Relative vorticity (solid, in 10^{-5} s^{-1}), divergence (dashed, in 10^{-5} s^{-1}), and vertical velocity (dotted, in 10^{-2} m s^{-1}) of the total wind on 1 Aug 1996. Profiles are for a 2° × 2° area centered on the MCV, averaged over 3 h ending at the times labeled. Data below 1750 m AMSL are not plotted. The levels of 0°C in the environment and of the tropopause are marked along the right side of each panel.

involves convergence. On 1 August 1996 that transition was facilitated by the MCV's vorticity, which reduced λ_R. At 0800 UTC, close to the time when a vortical circulation was first visible in loops of composite reflectivity, λ_R was 276 km, which is close to the 280 km calculated by Chen and Frank (1993) and the 300 km calculated by Cotton et al. (1989) for MCS environments. (Calculations of the Rossby radius are explained in section 2e.) By 1200 UTC, λ_R had shrunk to 136 km due to the increase in background vorticity. It stayed close to that value through 1500 UTC, the interval of maximum strengthening of the MCV. The radius of maximum wind we estimated for the MCV over multiple hours is 0.75°–1.50° latitude (83–167 km). The size of the stratiform region was difficult to measure precisely; the major axis was perhaps 350 km long during the asymmetric stage of the MCS, giving a pseudoradius of 175 km. This is slightly larger than λ_R, so a sizable fraction of the atmosphere's response to heating was retained near the MCS as convergent, vortical flow in the middle troposphere between 1200 and 1500 UTC. Rogers and Fritsch (2001) found a very similar relationship among preexisting vorticity, static stability, local Rossby radius, and vortex spinup in their simulation of a long-lived MCV.

In the MCS of 1 August 1996, tilting was the primary source of the positive, upper-tropospheric vorticity that further deepened the MCV during the final 3 h of the period of detailed analysis (Fig. 6f). Tilting and convergence were the primary sources of vorticity in the lower troposphere. Some of the strength of the MCV in the middle troposphere was maintained by effects represented by the residual and by convergence of absolute vorticity, because convergence, although weakening, continued from 6.5 to 11.0 km AMSL (Fig. 5c). Three-dimensional advection was generally a sink of vorticity at 6 km AMSL, the altitude of maximum vorticity in the MCV (Figs. 6e,f).

A few general properties of the vorticity budget for the total wind deserve mention. In agreement with observations by Chong and Bousquet (1999) and others, tilting and vertical advection of vorticity were very roughly anticorrelated about zero (Figs. 6b,d,f). Only

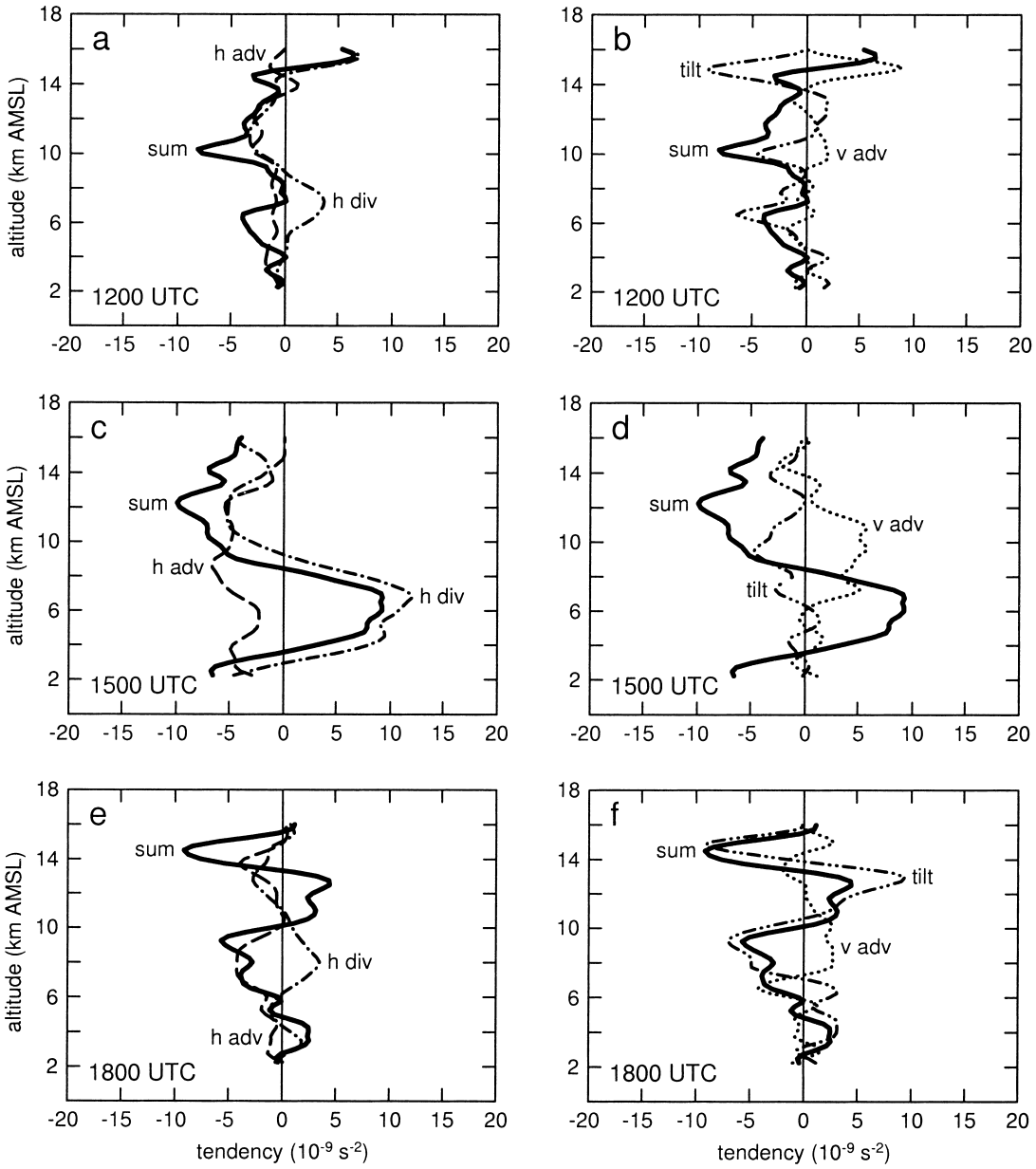

FIG. 6. Resolvable part of the vorticity budget for the total wind on 1 Aug 1996. (a), (c), (e) Horizontal advection (dashed) and horizontal divergence (dot–dashed). (b), (d), (f) Vertical advection (dotted) and tilting (dot–dot–dashed). The sum of all four terms (heavy solid) appears on each panel. Profiles are for a 2° × 2° area centered on the MCV, averaged over 3 h ending at the times labeled.

when this anticorrelation broke down did tilting and vertical advection play large, net roles in the local tendency. The often similar anticorrelation between horizontal advection and divergence of vorticity (e.g., Brandes and Ziegler 1993) was weaker, but still evident at times—in the lower and middle troposphere from 1500 to 1800 UTC, for example (Fig. 6e). Unresolved effects and observational errors represented by the residual were just as large as those explicitly resolved in the budget (cf. Figs. 6 and 7), which strongly suggests that regions of persistent convective-scale circulations significantly altered atmospheric vorticity on the mesoscale.

Much of the empirical research into this upscale communication of vorticity in masses of moist convection has focused on the large-scale effects of clusters of cumuli in the Tropics (e.g., Esbensen et al. 1982; Tollerud and Esbensen 1983; Sui and Yanai 1986). Figure 7 generally does not resemble profiles of residuals calculated for such tropical cloud clusters, but attempts to explain the lack of resemblance are beyond the scope of this paper.

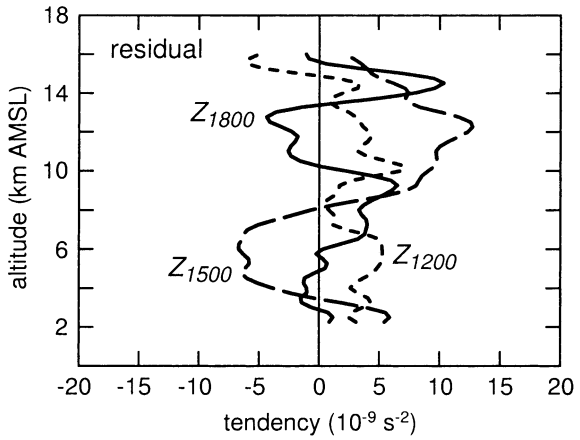

FIG. 7. Vorticity tendency due to the residual in the total wind at 1200 UTC (short dashed), 1500 UTC (long dashed), and 1800 UTC (solid) on 1 Aug 1996. Profiles are for a 2° × 2° area centered on the MCV, averaged over 3 h ending at the times labeled.

Upscale communication of vorticity has also been the subject of numerical studies. For example, in simulations by Montgomery and Enagonio (1998), clusters of cumulonimbi embedded within a vortex were able to strengthen a midtropospheric vortex through inward fluxes of angular momentum. The authors used potential vorticity to represent forcing by moist convection. In effect, the existing vortex was cyclonically accelerated because it assimilated positive potential vorticity and expelled negative potential vorticity. Because the magnitudes and distributions of potential vorticity realistically approximated both an MCV (radius of maximum wind was 200 km and midtropospheric tangential velocity was 5 m s^{-1}) and the moist convection near such a vortex, it is reasonable to assume that the results of Montgomery and Enagonio are relevant to MCVs such as that of 1 August 1996.

b. Discrimination between synoptic and mesoscale winds

When terms in the vorticity budget, (3), are itemized according to the synoptic background wind (terms with tildes) and the mesoscale perturbation to that background wind (terms with carets), the budget exemplifies commonly observed—in some cases defining—traits of synoptic and mesoscale motions. First, synoptic and mesoscale horizontal velocities were similarly large (Knievel and Johnson 2002), so contributions to vorticity from $\tilde{\mathbf{v}}(\tilde{u}, \tilde{v})$ and $\hat{\mathbf{v}}(\hat{u}, \hat{v})$ within the budget's terms were similarly large. Second, synoptic vertical velocity, $\tilde{w}$, was much smaller than mesoscale vertical velocity, $\hat{w}$, because synoptic divergence, $\nabla \cdot \tilde{\mathbf{v}}$, was much smaller than mesoscale divergence, $\nabla \cdot \hat{\mathbf{v}}$. Accordingly, terms in (3) with $\tilde{w}$ and $\nabla \cdot \tilde{\mathbf{v}}$ contributed very little to the budget. Third, as long as planetary vorticity, f, is considered part of synoptic vorticity, synoptic and mesoscale vorticities, $\tilde{\zeta} + f$ and $\hat{\zeta}$, were of the same magnitude, and in some terms contributed large values to the budget. Gradients in synoptic vorticity were much smaller than gradients in mesoscale vorticity, though. Finally, shears in synoptic and mesoscale winds were similarly large, so tilting of both $\tilde{\boldsymbol{\eta}}(\tilde{\xi}, \tilde{\eta})$ and $\hat{\boldsymbol{\eta}}(\hat{\xi}, \hat{\eta})$ contributed similarly large values to vorticity tendency. The term-by-term analysis of the vorticity budget in the following sections makes these generalities more meaningful.

1) TENDENCY FROM HORIZONTAL ADVECTION

Nearly all the vorticity tendency from horizontal advection was due to advection of mesoscale vorticity by the synoptic wind (Fig. 8). The reason horizontal advection of mesoscale vorticity by the mesoscale wind was so small is that, in the predominantly vortical flow of the MCV, the largest component of the mesoscale wind tended to be orthogonal to the gradient of meso-

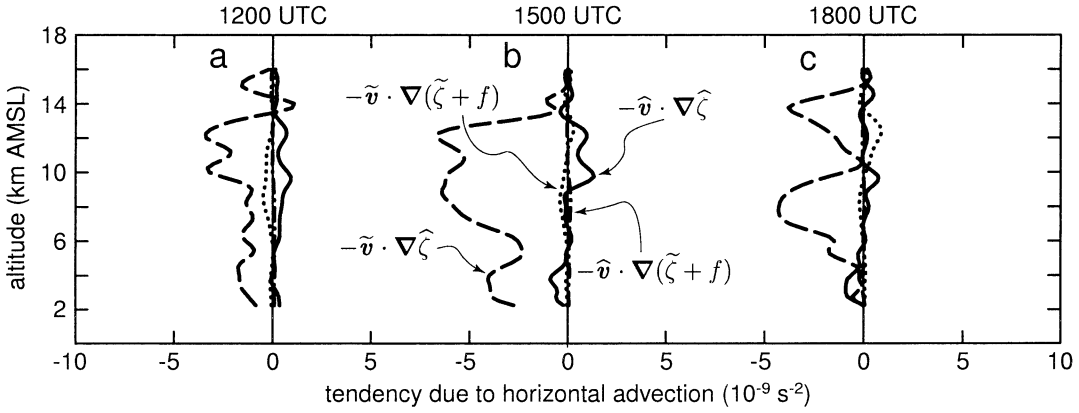

FIG. 8. Vorticity tendency due to components of horizontal advection on 1 Aug 1996. Terms are as follows: advection of mesoscale perturbation in vorticity by the mesoscale perturbation in wind (solid) and by the synoptic wind (dashed), and advection of synoptic vorticity by the mesoscale perturbation in wind (dashed–dotted) and by the synoptic wind (dotted). Profiles are for a 2° × 2° area centered on the MCV, averaged over 3 h ending at the times labeled.

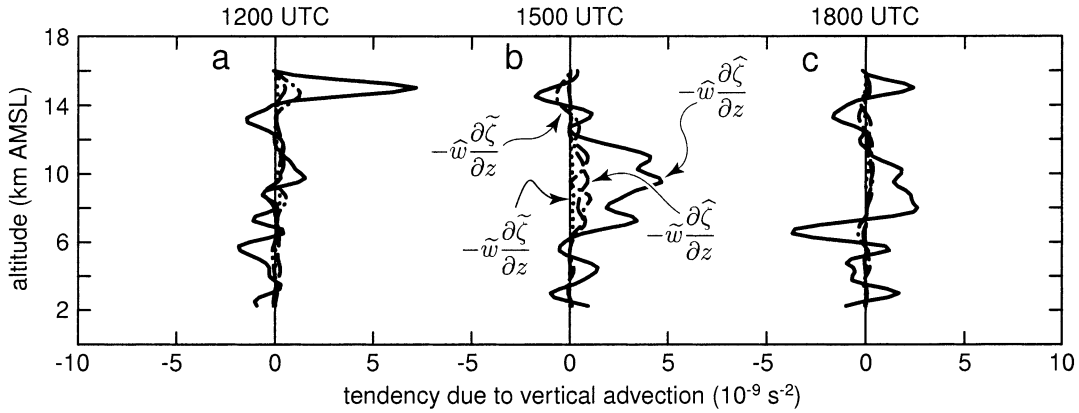

FIG. 9. Vorticity tendency due to components of vertical advection on 1 Aug 1996. Terms are as follows: advection of mesoscale perturbation in vorticity by the mesoscale perturbation in wind (solid) and by the synoptic wind (dashed), and advection of synoptic vorticity by the mesoscale perturbation in wind (dashed–dotted) and by the synoptic wind (dotted). Profiles are for a 2° × 2° area centered on the MCV, averaged over 3 h ending at the times labeled.

scale vorticity [evident in Fig. 4 of Knievel and Johnson (2002)], so the dot product in the horizontal advection term was small even though the vectors in the term were large. Gradients of synoptic vorticity were too small to permit much horizontal advection, even though synoptic vorticity was as large as mesoscale vorticity because we included planetary vorticity in the former.

Because larger vertical shears generally lead to shorter-lived MCVs, differential advection seems to be one mechanism that destroys the vortices (Trier et al. 2000). Figure 8 suggests that such differential advection is mostly by environmental wind, not by wind within the mesoscale circulations of MCSs. In the case of the MCV we studied, this differential advection arose not simply because of the horizontal translation of vertically varying mesoscale vorticity, but also because of vertically varying horizontal synoptic wind. [See Fig. 9 of Knievel and Johnson (2002) for depictions of the synoptic wind.]

2) TENDENCY FROM VERTICAL ADVECTION

Nearly all the vorticity tendency from vertical advection was due to advection of mesoscale vorticity by the mesoscale wind (Fig. 9). Not surprisingly, the only vertical motions strong enough to contribute much to vertical advection were in the mesoscale field. Synoptic vorticity, while large, did not lead to large vertical advection even by the mesoscale wind because vertical gradients of synoptic vorticity were small.

3) TENDENCY FROM DIVERGENCE

No component in the vorticity tendency from horizontal divergence was negligibly small, although two of the four components were dominant (Fig. 10). From 1200 to 1500 UTC, when the MCV underwent the greatest deepening and strengthening, vorticity in the MCV

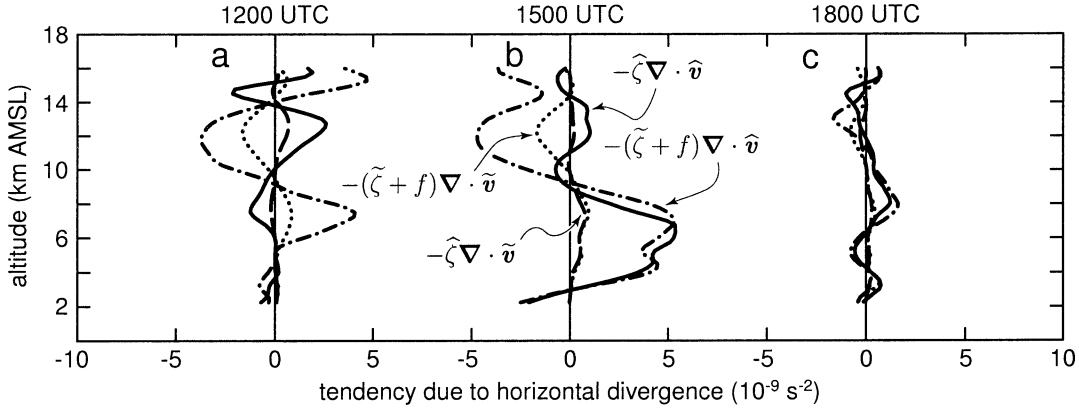

FIG. 10. Vorticity tendency due to components of horizontal divergence on 1 Aug 1996. Terms are as follows: divergence of mesoscale perturbation in vorticity by the mesoscale perturbation in wind (solid) and by the synoptic wind (dashed), and divergence of synoptic vorticity by the mesoscale perturbation in wind (dashed–dotted) and by the synoptic wind (dotted). Profiles are for a 2° × 2° area centered on the MCV, averaged over 3 h ending at the times labeled.

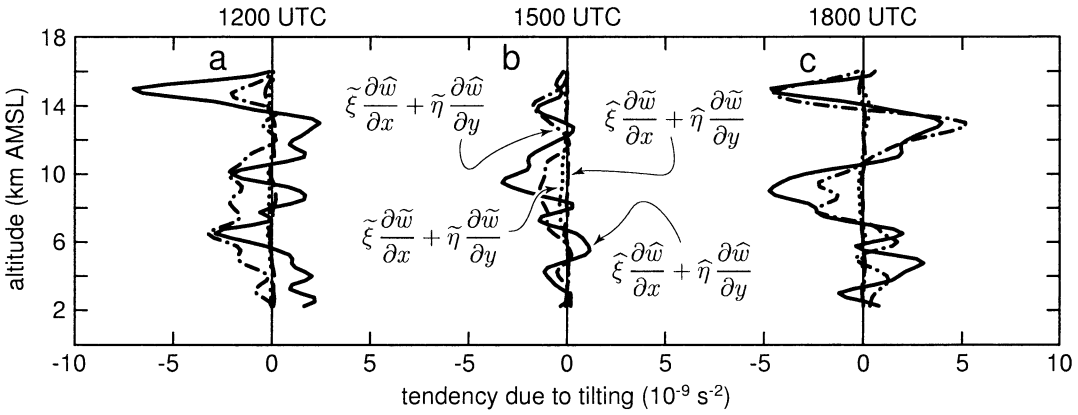

FIG. 11. Vorticity tendency due to components of tilting on 1 Aug 1996. Terms are as follows: tilting of vertical shear of the mesoscale perturbation in wind by the horizontal gradient of mesoscale perturbation in vertical motion (solid) and by the horizontal gradient of synoptic vertical motion (dashed), and tilting of vertical shear of the synoptic wind by the horizontal gradient of mesoscale perturbation in vertical motion (dashed–dotted) and by the horizontal gradient of synoptic vertical motion (dotted). Profiles are for a $2° \times 2°$ are centered on the MCV, averaged over 3 h ending at the times labeled.

was generated mostly, and nearly equally, by convergence of mesoscale vorticity and convergence of synoptic vorticity, both by the mesoscale wind. Tendency due to convergence of synoptic vorticity by the synoptic wind was at least a factor of 1/2 smaller than the dominant terms, and tendency due to convergence of mesoscale vorticity by the synoptic wind was slightly smaller yet, especially in the upper troposphere.

It is through convergence that vorticity from shortwave troughs near an MCS would play a role in generating an MCV. The size of a typical shortwave trough would put its vorticity into both the synoptic and mesoscale regimes, as we have approximated them. According to the general conclusions one can draw from Fig. 10, the primary concentrator of vorticity in shortwave troughs is probably the mesoscale wind.

4) TENDENCY FROM TILTING

Finally, the only two components that contributed appreciably to the vorticity tendency from tilting were tilting of both synoptic and mesoscale vorticity by horizontally varying mesoscale up- and downdrafts (Fig. 11). Synoptic drafts were too weak, and their horizontal variations too small, to significantly tilt tubes of horizontal vorticity. Tilted horizontal vorticity consistently contained large synoptic as well as mesoscale components. This differs somewhat from the study by Davis and Weisman (1994), in which they found that tilting of environmental shear was dominant early in a simulated line-end mesoscale vortex within an MCS, but was later exceeded by tilting of perturbation vorticity. However, no one has definitively established that the cyclonic member of a pair of line-end vortices and an MCV of the kind studied herein are precisely the same phenomenon.

5. Comparison between two forms of the vorticity budget

For the vorticity budget we used the conventional form of the vorticity equation, (1), for two reasons. First, the conventional form has explicit terms for advection, divergence, and tilting, so one can easily grasp the physical processes represented. Second, the great majority of other vorticity budgets for observed MCVs are based on the conventional form (e.g., Johnson and Bartels 1992; Brandes and Ziegler 1993; Keenan and Rutledge 1993; Scott and Rutledge 1995; Chong and Bousquet 1999; Bousquet and Chong 2000), so it is easy to put our results in a larger context.

However, as explained in section 2d, the local tendency in the conventional form of the vorticity equation is very sensitive to the character of spatial derivatives because it is the sum of four large terms that often nearly cancel one another. To assess how much our primary results depend on our choice of vorticity equation, we tested a second budget using the divergence, or the flux, form of the vorticity equation, (4)–(6).

The two methods produced grossly similar resolved tendencies, but with noteworthy differences in the details (Fig. 12). In the lower 65% of the troposphere, below about 8 km AMSL, the two budgets agree well, although the divergence form tended to produce slightly larger tendencies. In the upper troposphere, the divergence form produced significantly larger tendencies. In a few layers, such as between 8 and 11 km AMSL at 1500 UTC (Fig. 12b), the two budgets even produced tendencies of opposite sign. However, throughout much of the troposphere, the signs of the vertical derivative of tendency were virtually identical between the budgets, as were the altitudes of local extrema. Many of the most general conclusions one might draw from the

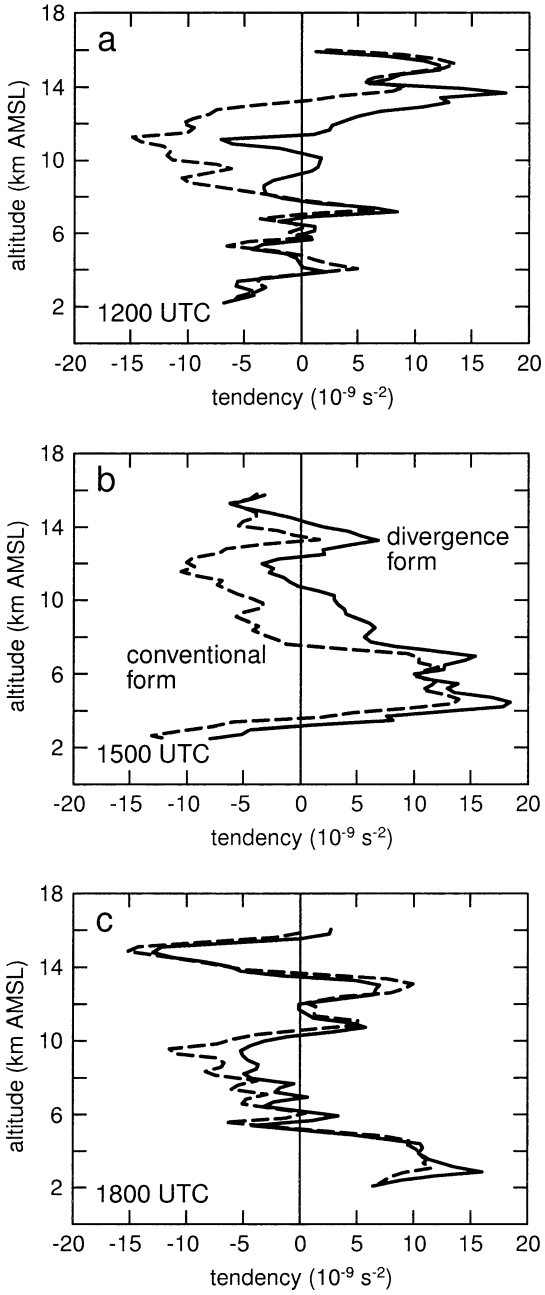

FIG. 12. Resolved part of the local tendency of relative vorticity calculated according to the conventional (dashed) and divergence (solid) forms of the budget. Profiles are at (a) 1200, (b) 1500, and (c) 1800 UTC on 1 Aug 1996 for a 2° × 2° area centered on the MCV in the middle troposphere; the profiles have not been otherwise averaged or smoothed.

vertical structure of the resolved tendency, if not its actual value at a given altitude, in our case seem to be largely independent of the form of the budget used.

There are at least two reasons for the differences between the resolved tendencies from the divergence and conventional forms of the budget. First, the divergence form of the vorticity equation, (4)–(6), has fewer terms (and fewer derivatives) than the conventional form, (1), so there are fewer calculations. Second, and almost certainly more crucial, the terms in the two budgets are not calculated at an identical set of grid points. Because the divergence form involves a vector with no vertical component, an areally averaged budget is calculated simply by applying (6) at the grid points along the perimeter of the area in question. The divergence form is unaffected by vorticity extrema inside the perimeter. However, the conventional form of the budget *is* affected by extrema inside the perimeter because terms in the budget are calculated at every grid point, then the results are averaged.

Fortunately, the differences between the divergence and conventional forms of the budget do not call into question the primary results of this study. First, the mesoscale and synoptic components of wind contributed significant vorticity to the MCV of 1 August 1996; the former mainly through convergence, vorticity, and three-dimensional wind; the latter mainly through planetary vorticity and horizontal wind. Second, the two largest net, resolved sources of vorticity were convergence and tilting, the prominence of which varied during the lifetime of the MCV. Mesoscale convergence of mesoscale and synoptic vorticity produced the single biggest increase in the maturing MCV's strength. Most of the tendency due to tilting was from mesoscale up- and downdrafts acting on horizontal synoptic and mesoscale vorticity.

6. Synthesis

We presented a scale-discriminating vorticity budget of a mesoscale convective vortex (MCV) generated by a mesoscale convective system (MCS). The MCS, which comprised a leading convective line and trailing stratiform region, traversed Kansas and Oklahoma on 1 August 1996 and displayed many of the features in radar reflectivity common to systems that generate MCVs.

Because the MCS matured, decayed, and dissipated in the National Oceanic and Atmospheric Administration (NOAA) Wind Profiler Network (NPN), we were able to analyze sources and sinks of vorticity in the MCV over 9 h on scales between those of semidaily operational rawinsondes and Doppler radars. We used a Barnes bandpass filter to divide observed wind into a component that was predominantly synoptic background wind and a component that was predominantly a mesoscale perturbation to that background wind.

The most important result from the vorticity budget is that both the synoptic background wind and the mesoscale perturbation in wind contributed significant vorticity to the MCV of 1 August 1996. Vorticity tendency from horizontal advection was due almost entirely to advection of mesoscale vorticity by the synoptic wind. Tendency from vertical advection was due almost entirely to advection of mesoscale vorticity by the mesoscale wind. The largest contribution to vorticity ten-

dency from divergence was due to convergence of both synoptic and mesoscale vorticity by the mesoscale wind. Finally, only the horizontal variation of up- and downdrafts in the mesoscale wind contributed appreciably to tilting horizontal vorticity, and this horizontal vorticity was in the vertical shear of both the synoptic wind and the mesoscale wind.

If the MCV of 1 August 1996 is representative, the results herein suggest that completely realistic simulations of MCVs should include planetary vorticity and a plausible, three-dimensionally heterogeneous background wind. However, an observational study such as this does not clearly establish precisely in what ways an MCV is sensitive to heterogeneity in the environment. Studies involving numerical simulations are better suited to that question.

Acknowledgments. The bulk of this research was conducted while the first author was at Colorado State University and was supported by the National Science Foundation and the National Aeronautics and Space Administration under the respective Grants ATM 9618684 and NCC5-288 SUPP 0002. The remainder, conducted while the first author was at the National Severe Storms Laboratory working under D. P. Jorgensen, was supported through an associateship awarded by the National Research Council.

Profiler data and code to read them are from S. B. Trier and C. F. Shih of the National Center for Atmospheric Research (NCAR); WSI's NOWrad radar reflectivity is from the Global Hydrology Resource Center; and GCIP/ESOP-96 data are from the Joint Office for Scientific Support of the University Corporation for Atmospheric Research and the National Oceanic and Atmospheric Administration (NOAA).

Contributions from the following people improved our research and writing: C. A. Davis and S. B. Trier of NCAR; J. E. Nachamkin of the Naval Research Laboratory; E. I. Tollerud of the Forecast Systems Laboratory; J. P. Kossin of the Space Science and Engineering Center; P. T. Haertel of the NOAA/Aeronomy Laboratory; M. D. Parker of the University of Nebraska; P. C. Ciesielski, W. R. Cotton, M. T. Montgomery, and J. A. Ramirez of Colorado State University (CSU); and three anonymous reviewers. M. D. Parker, in particular, was extremely helpful. R. K. Taft of CSU provided invaluable computer support.

REFERENCES

Barnes, S. L., 1973: Mesoscale objective analysis using weighted time-series observations. NOAA Tech. Memo. ERL NSSL-62, 60 pp. [Available from National Severe Storms Laboratory, Norman, OK 73069.]

Bartels, D. L., and R. A. Maddox, 1991: Midlevel cyclonic vortices generated by mesoscale convective systems. *Mon. Wea. Rev.,* **119,** 104–118.

Biggerstaff, M. I., and R. A. Houze Jr., 1991: Kinematic and precipitation structure of the 10–11 June 1985 squall line. *Mon. Wea. Rev.,* **119,** 3034–3065.

Bousquet, O., and M. Chong, 2000: The oceanic mesoscale convective system and associated mesovortex observed 12 December 1992 during TOGA–COARE. *Quart. J. Roy. Meteor. Soc.,* **126,** 189–211.

Brandes, E. A., 1990: Evolution and structure of the 6–7 May 1985 mesoscale convective system and associated vortex. *Mon. Wea. Rev.,* **118,** 109–127; Corrigendum, **118,** 990.

——, and C. L. Ziegler, 1993: Mesoscale downdraft influences on vertical vorticity in a mature mesoscale convective system. *Mon. Wea. Rev.,* **121,** 1337–1353.

Brock, F. V., K. C. Crawford, R. L. Elliott, G. W. Cuperus, S. J. Stadler, H. L. Johnson, and M. D. Eilts, 1995: The Oklahoma Mesonet: A technical overview. *J. Atmos. Oceanic Technol.,* **12,** 5–19.

Ceselski, B. F., and L. L. Sapp, 1975: Objective wind field analysis using line integrals. *Mon. Wea. Rev.,* **103,** 89–100.

Chen, S. S., and W. M. Frank, 1993: A numerical study of the genesis of extratropical convective mesovortices. Part I: Evolution and dynamics. *J. Atmos. Sci.,* **50,** 2401–2426.

Chong, M., and O. Bousquet, 1999: A mesovortex within a near-equatorial mesoscale convective system during TOGA COARE. *Mon. Wea. Rev.,* **127,** 1145–1156.

Cotton, W. R., M. S. Lin, R. L. McAnelly, and C. J. Tremback, 1989: A composite model of mesoscale convective complexes. *Mon. Wea. Rev.,* **117,** 765–783.

Cram, T. A., M. T. Montgomery, and R. F. A. Hertenstein, 2002: Early evolution of vertical vorticity in a numerically simulated idealized convective line. *J. Atmos. Sci.,* **59,** 2113–2127.

Davis, C. A., and M. L. Weisman, 1994: Balanced dynamics of mesoscale vortices produced in simulated convective systems. *J. Atmos. Sci.,* **51,** 2005–2030.

Durran, D. R., and J. B. Klemp, 1982: On the effects of moisture on the Brunt–Väisälä frequency. *J. Atmos. Sci.,* **39,** 2152–2158.

Esbensen, S. K., 1993: Cumulus effects on vorticity. *The Representation of Cumulus Convection in Numerical Models, Meteor. Monogr.,* No. 46, Amer. Meteor. Soc., 93–98.

——, E. I. Tollerud, and J.-H. Chu, 1982: Cloud-cluster-scale circulations and the vorticity budget of synoptic-scale waves over the eastern Atlantic intertropical convergence zone. *Mon. Wea. Rev.,* **110,** 1677–1692.

Frank, W. M., 1983: The cumulus parameterization problem. *Mon. Wea. Rev.,* **111,** 1859–1871.

Fritsch, J. M., J. D. Murphy, and J. S. Kain, 1994: Warm-core vortex amplification over land. *J. Atmos. Sci.,* **51,** 1780–1807.

Gallus, W. A., Jr., and R. H. Johnson, 1992: The momentum budget of an intense midlatitude squall line. *J. Atmos. Sci.,* **49,** 422–450.

Hertenstein, R. F. A., and W. H. Schubert, 1991: Potential vorticity anomalies associated with squall lines. *Mon. Wea. Rev.,* **119,** 1663–1672.

Houze, R. A., Jr., S. A. Rutledge, M. I. Biggerstaff, and B. F. Smull, 1989: Interpretation of Doppler weather radar displays of midlatitude mesoscale convective systems. *Bull. Amer. Meteor. Soc.,* **70,** 608–619.

Johnson, R. H., and D. L. Bartels, 1992: Circulations associated with a mature-to-decaying midlatitude mesoscale convective system. Part II: Upper-level features. *Mon. Wea. Rev.,* **120,** 1301–1320.

Keenan, T. D., and S. A. Rutledge, 1993: Mesoscale characteristics of monsoonal convection and associated stratiform precipitation. *Mon. Wea. Rev.,* **121,** 352–374.

Knievel, J. C., and R. H. Johnson, 2002: The kinematics of a midlatitude, continental mesoscale convective system and its mesoscale vortex. *Mon. Wea. Rev.,* **130,** 1749–1770.

Koch, S. E., M. DesJardins, and P. J. Kocin, 1983: An interactive Barnes objective map analysis scheme for use with satellite and conventional data. *J. Climate Appl. Meteor.,* **22,** 1487–1503.

Maddox, R. A., 1980: An objective technique for separating mac-

roscale and mesoscale features in meteorological data. *Mon. Wea. Rev.,* **108,** 1108–1121.
Mapes, B. E., 1993: Gregarious tropical convection. *J. Atmos. Sci.,* **50,** 2026–2037.
Menard, R. D., and J. M. Fritsch, 1989: A mesoscale convective complex-generated inertially stable warm core vortex. *Mon. Wea. Rev.,* **117,** 1237–1261.
Montgomery, M. T., and J. Enagonio, 1998: Tropical cyclogenesis via convectively forced vortex Rossby waves in a three-dimensional quasigeostrophic model. *J. Atmos. Sci.,* **55,** 3176–3207.
O'Brien, J. J., 1970: Alternative solutions to the classical vertical velocity problem. *J. Appl. Meteor.,* **9,** 197–203.
Raymond, D. J., and H. Jiang, 1990: A theory for long-lived mesoscale convective systems. *J. Atmos. Sci.,* **47,** 3067–3077.
Reed, R. J., and R. H. Johnson, 1974: A vorticity budget of synoptic wave disturbances in the tropical western Pacific. *J. Atmos. Sci.,* **31,** 1784–1790.
Rogers, R. F., and J. M. Fritsch, 2001: Surface cyclogenesis from convectively driven amplification of midlevel mesoscale convective vortices. *Mon. Wea. Rev.,* **129,** 605–637.
Schubert, W. H., and J. J. Hack, 1982: Inertial stability and tropical cyclone development. *J. Atmos. Sci.,* **39,** 1687–1697.
——, ——, P. L. Silva Dias, and S. R. Fulton, 1980: Geostrophic adjustment in an axisymmetric vortex. *J. Atmos. Sci.,* **37,** 1464–1484.
Scott, J. D., and S. A. Rutledge, 1995: Doppler radar observations of an asymmetric MCS and associated vortex couplet. *Mon. Wea. Rev.,* **123,** 3437–3457.
Skamarock, W. C., M. L. Weisman, and J. B. Klemp, 1994: Three-dimensional evolution of simulated long-lived squall lines. *J. Atmos. Sci.,* **51,** 2563–2584.
Sui, C.-H., and M. Yanai, 1986: Cumulus ensemble effects on the large-scale vorticity and momentum fields of GATE. Part I: Observational evidence. *J. Atmos. Sci.,* **43,** 1618–1642; Corrigendum, **46,** 1630.
Tollerud, E. I., and S. K. Esbensen, 1983: An observational study of the upper-tropospheric vorticity fields in GATE cloud clusters. *Mon. Wea. Rev.,* **111,** 2161–2175.
Trier, S. B., C. A. Davis, and W. C. Skamarock, 2000: Long-lived mesoconvective vortices and their environment. Part II: Induced thermodynamic destabilization in idealized simulations. *Mon. Wea. Rev.,* **128,** 3396–3412.
Weisman, M. L., and C. A. Davis, 1998: Mechanisms for the generation of mesoscale vortices within quasi-linear convective systems. *J. Atmos. Sci.,* **55,** 2603–2622.
Zhang, D.-L., 1992: The formation of a cooling-induced mesovortex in the trailing stratiform region of a midlatitude squall line. *Mon. Wea. Rev.,* **120,** 2763–2785.
——, and J. M. Fritsch, 1988: A numerical investigation of a convectively generated, inertially stable, extratropical warm-core mesovortex over land. Part I: Structure and evolution. *Mon. Wea. Rev.,* **116,** 2660–2687.